ANL-HEP-PR--81-24

DE82 012895

ANL-HEP-PR-81-24
PU-81-494
CMU-COO-3066-173

Strange-Particle Production in High-Energy $\bar{\nu}$ and ν Charged-Current Interactions on Protons

R. Brock[a)], S. J. Barish[b)], A. Engler, T. Kikuchi, R. W. Kraemer, F. Messing, B. J. Stacey[c)], and M. Tabak[d)]

Carnegie-Mellon University, Pittsburgh, PA 15213

M. Derrick, P. Gregory[e)], F. LoPinto[f)], B. Musgrave, J. Schlereth, P. Schreiner[f)], and R. Singer[f)]

Argonne National Laboratory, Argonne, IL 60439

V. E. Barnes, T. S. Carman, D. D. Carmony, C. Davis, E. Fernandez[g)], A. F. Garfinkel, and A. T. Laasanen

Purdue University, W. Lafayette, IN 47907

(Received

We have studied the semi-inclusive reactions $\bar{\nu}p \rightarrow \mu^+V^oX$ and $\nu p \rightarrow \mu^-V^oX$, and measured the fractional rate for producing one or more neutral strange particles in these reactions to be 0.16 ± 0.03 and 0.15 ± 0.04, respectively. We have observed $K^-(892)$ and $\Sigma^-(1385)$ production in $\bar{\nu}p$ scattering at a few percent of the inclusive rate. No evidence for D^o production was seen in the $K^o_s\pi^+\pi^-$ final state. The distributions in the standard

MGU

deep-inelastic kinematic variables are presented for events with strange particles and compared to those for the other charged current data. The fragmentation properties of events containing a K_s^o are in agreement with results from electroproduction experiments, and we have measured $\int_{0.3}^{1.0} \frac{1}{N_T} \frac{dN}{dz} dz = 0.029 \pm 0.005$, which is smaller than the prediction of the Field and Feynman fragmentation model.

I. Introduction

We report here the results of $\bar{\nu}p$ and νp scattering in which the final states include at least one visible neutral strange particle, K_s^o and/or Λ. The production of strange particles by the weak interaction is interesting on several counts and, in particular, provides a signal for the production of new quantum numbers. Accordingly, our earlier analysis[1] of the x and y distributions of the $\bar{\nu}p$ charged-current events containing strange particles showed that charmed-particle production via the process $\bar{\nu}_\mu \bar{s} \to \mu^+ \bar{c}$ is required. A further conclusion was that a significant left-handed component was needed for the $\binom{c}{s}$ doublet. We now present a more detailed discussion of the experimental techniques used in the data selection.

The events with strangeness are compared to the inclusive charged-current event sample using the standard inclusive kinematic variables[2]. We also present the invariant mass distributions and inclusive fragmentation distributions. In the Appendix, we discuss the Monte Carlo (MC) simulation of the events with strange particles which led to our algorithm for determining the neutrino energy.

II. Event Selection and Beam Energy Determination

The pictures for this experiment were taken in three separate exposures[3] of the 15-foot bubble chamber, filled with liquid hydrogen, to the horn-focussed, wide-band antineutrino beam at Fermilab. A total of 208K pictures were taken of which 184K were with a proton energy of 400 GeV and an average intensity on target of 1.4×10^{13} protons per pulse. The calculated ν and $\bar{\nu}$ flux spectra for the experiment are shown in Fig. 1.[3]

The pictures were scanned at each of the three institutions with events selected according to the following rules:

1. Three views were scanned, but events visible in only two views were also recorded.
2. Only events having three or more charged tracks[4] were recorded, since the efficiency for finding one-prong events was low. Events were discarded if (a) they had two stopping positive tracks, (b) the sum of the momenta of the charged tracks in the forward hemisphere was less than 2 GeV/c, or (c) they had a non-decaying or non-kinking track traveling in a backward cone of 45° with respect to the beam direction.
3. All secondary neutral vertices were recorded.
4. Events which appeared to originate in the wall of the bubble chamber were flagged as such.

Topology-dependent scanning efficiencies were calculated from a double scan and are given in Table I. The average scanning efficiency was 96% for events with strange particles. The events found were examined by a physicist who prepared measurement instructions.

Geometrical reconstruction utilized a version of the Three-View Geometry Program (TVGP) modified for the 15-foot bubble chamber. The multiplicity-dependent reconstruction efficiencies for the inclusive sample are shown in Table I. Backgrounds due to incident K_L^o and neutrons were eliminated by imposing a cut at 5 GeV/c on the visible momentum.[5] The events were required to be inside an 18.7 m^3 fiducial volume which ensured a minimum track length of 30 cm to the downstream chamber wall.

Events selected as described above were classified as V's (unambiguous strange particle decays), G's (unambiguous gamma-ray conversions), and A's (ambiguous between V and G). Following geometrical reconstruction, events were kinematically fit to γ, K_S^o, and Λ hypotheses; the total numbers of γ's, K_S^o, and Λ's found are given in Table II. The table also indicates the degree of ambiguity between the various hypotheses.[4] The ambiguities were resolved by the usual techniques depending on the kinematical differences between strange particle decays and γ-conversions. The final event ambiguity resolution is also summarized in Table II. In order to obtain a pure strange particle sample, the final ~ 1% of events remaining ambiguous with γ-conversions, were classified as photon conversions.

A minimum flight path of 1 cm was required for the neutral particle because of the difficulty of detecting a decay or conversion close to the primary event vertex. The mean lifetimes of the resulting K_S^o and Λ^o samples were found to be $(0.892 \pm 0.002) \times 10^{-10}$ sec and $(2.63 \pm 0.02) \times 10^{-10}$ sec, respectively, and are in satisfactory agreement with the known values.

Each event was classified as either a $\bar{\nu}$ charged-current ($\overline{CC}$) candidate, or a ν charged-current (CC) candidate, or as a neutral current (NC) candidate. These assignments were accomplished by the use of a kinematic algorithm for the selection of the muon[3] and resulted in a raw data sample of 2142 $\overline{CC}$ and 621 CC events. A Monte Carlo study of the muon selection technique showed that, after the selections on the kinematic variables x and y listed below, the efficiency for $\overline{CC}$ (CC) event assignments was 97% (82%), while the background of misclassified $\overline{CC}$ (CC) events was 7% (15%).

A total weight, w, was applied to each strange particle event with multiplicity i and is given by:

$$w = w(\text{strange}) \times w_i(\text{inclusive})$$

where w(strange) corrects for the scanning, reconstruction, and fitting efficiencies for the V, and also for the minimum neutral particle path length and its escape loss, and w_i(inclusive) corrects the equivalent inefficiencies in the inclusive sample. The combined corrections resulted in an average weight of 1.6 for events containing a strange particle. The corrections for the neutral decay modes are not included in this total weight but were applied to our results.

Since the beam energy determination was carried out somewhat differently for the strange particle events than for the inclusive sample, we briefly describe the technique used. We assumed that the longitudinal momentum (P_L) of the neutral hadronic system is correlated with the (measurable) neutral transverse momentum (P_T) in the same way as for the charged hadronic system. The results for this correlation are shown in Fig. 2. The appropriate momentum vectors are given in Fig. 3. The correlation data, shown in Fig. 2, exhibit a linear form with two well-defined regions. This variation provides us with a measure of the longitudinal momentum of the neutral system, and hence the incident neutrino energy. The correlation is, quantitatively,

$$P_L = 2.5\ P_T + 0.4 \text{ for } P_T < 0.8 \text{ GeV/c}$$

and

$$P_L = 4.25\ P_T - 1.0 \text{ for } P_T > 0.8 \text{ GeV/c} \quad .$$

The same, simple technique was applied to events with a visible strange particle. However, for events with an observed strange particle, it is reasonable to assume that significant momentum is often carried away by a second unobserved strange particle. Hence, the P_L-P_T correlation would be different in this case, and the use of the above parameterization, which is appropriate to π^o's, would underestimate the neutrino energy.

We have studied this problem with the MC program described in the Appendix. The resulting parameterization which was used for events containing one visible strange particle is $P_L = 4\ P_T + 0.4$. The agreement with the data from the strange particle event sample is good, and, as shown in the Appendix, this parameterization leads to resolutions for events containing strange particles very similar to those of the inclusive sample.

Table III gives the observed and corrected number of strange particle events for reactions of the type:

$$\bar{\nu}p \rightarrow \mu^+ V^o X,$$

$$\bar{\nu}p \rightarrow \mu^+ V_1^o V_2^o X,$$

$$\nu p \rightarrow \mu^- V^o X,$$

$$\nu p \rightarrow \mu^- V_1^o V_2^o X,$$

where X denotes all hadrons, except V's, from the primary vertex. The corrected event numbers in Table III include the unseen neutral decay modes, in addition to the weights discussed earlier. The events have also been selected to have $E_\nu > 5.0$ GeV, $W > 1.0$ GeV, $0.05 < x < 1.0$, and $0.1 < y < 0.8$. The rate for $\overline{CC}$ events containing at least one V^o is

$$\frac{(\bar{\nu}p \rightarrow \mu^+V^oX^o + \bar{\nu}p \rightarrow \mu^+V_1^oV_2^oX^o)}{\bar{\nu}p \rightarrow \mu^+X^o} = 0.16 \pm 0.03 \quad ,$$

and for CC events the rate is

$$\frac{(\nu p \rightarrow \mu^-V^oX^{++} + \nu p \rightarrow \mu^-V_1^oV_2^oX^{++})}{\nu p \rightarrow \mu^-X^{++}} = 0.15 \pm 0.04 \quad .$$

For the $\bar{\nu}p$ data, the one-prong events, with an all neutral hadronic system, are not included either in the numerator or the denominator. About 14% of the inclusive sample has a one-prong topology. We observe only two events that can be ascribed to the exclusive final state $\mu^+\Lambda$ which corresponds to a cross section of $\sim 0.6 \cdot 10^{-40}$ cm^2.

The partial cross sections for the events with a single V^o, μK^oX, and $\mu\Lambda(\Sigma^o)X$, given in Table III, have been corrected to exclude the contributions from the final states $\mu K^o\bar{K}^oX^o$ and $\mu\bar{K}^o\Lambda(\Sigma^o)X^o$. These corrections are made from the observed $K^o\bar{K}^o$ and $K^o\Lambda^o(\Sigma^o)$ events.

Our measurement of the $\bar{\nu}p \rightarrow \mu^+V^oX$ rate is the first such measurement on a simple target and agrees with the rate for $\bar{\nu}$ neon scattering.[6] Also, our measurement of the rate for $\nu p \rightarrow \mu^-V^oX$ agrees with other measurements of this reaction.[7,8] The rates for strange particle production from these experiments are compared in Table IV.

III. Properties of Strange Particle Production

We show first the distributions (corrected for efficiencies as described in Section II) in the usual kinematical quantities for the charged current events with strange particles. These are contained in Figs. 5 through 10 with, in each case, (a) showing the $\overline{CC}$ data and (b) showing the CC data. The curves show for comparison the distribution of the inclusive events normalized to the number of strange particle events.

The $\overline{CC}$ strange particle events are clearly produced at lower x values than their inclusive counterparts. We have shown that this behavior can be explained by the $\bar{s} \rightarrow \bar{c}$ transition leading to charmed particles which subsequently decay predominantly to strange particles.[1] There are no obvious differences between the x distributions of strange particle events and the CC inclusive sample; this is consistent with the roughly equal production of charm from the valence and sea quarks.

Figure 11 shows the visible strange particle rate as a function of W using results from several neutrino experiments,[6-10] as well as muon production[11] and photoproduction[12]. It is interesting to note that the $\bar{\nu}$ points are typically higher at fixed W than the ν values which can be attributed to the different mechanisms for charm production.

The distributions in Feynman x for the K^o's and Λ's show that the Λ hyperons are produced predominantly in the backward hemisphere with a F/B ratio of 0.22 ± 0.08, whereas the K^o's are more forward with $F/B = 2.11 \pm 0.46$.[13]

Mass distributions for all $\Lambda\pi^\pm$ and $K^o_s\pi^\pm$ combinations are shown in Figs. 12 through 15. All positively charged tracks are assumed to be pions unless identified as protons by ionization. There are clear signals for both the $K^{-}(892)$ and the $\Sigma^{-}(1385)$, but no signal for the $\Sigma^{+}(1385)$ and at best a broad enhancement in the 850–900 MeV region of the $\overline{CC}$ $K_s^o\pi^+$ effective mass distribution. The $K^{-}(892)$ signal of approximately 14 combinations corresponds to a production rate of (4 ± 2)% of the total $\overline{CC}$ inclusive sample above the $K^*\Lambda$ kinematic threshold. This is in agreement with the $K^+(890)$ rate measured in νp interactions.[8] The $\Sigma^{-}(1385)$ signal in $\overline{CC}$ events of roughly 16 combinations above background is about 2% of the total $\overline{CC}$ sample. Each pion appears only once in combination with a K_s^o or Λ in the signal region in either the positive or negative channels. The curve in the $\overline{CC}$ $K_s^o\pi^-$ plot is the normalized distribution from the $K_s^o\pi^+$ plot as an estimate of the combinatorial background.

Figure 16 shows the $K_s^o\pi^+\pi^-$ mass distribution for $\overline{CC}$ events. There is no signal above background in the D-meson region. Based on the known $D^o \to K^o\pi^+\pi^-$ branching ratio of (3.8 ± 1.2)% and our measured inclusive charm meson production rate of approximately 5%, we expect, at most, only four events above background.

Figs. 17 and 18 show the fully corrected distributions in the quantity $z = E_{HAD}/\nu$ for K_s^o or Λ^o events. The curves in Fig. 17(a) show the predicted distributions for two descriptions of d, $\bar{u}$, and s quarks fragmenting into non-charmed mesons. The dashed curve shows the result of the Field and Feynman (FF)[14] parameterization and the solid curve shows the predictions of Sehgal.[15] In the solid curve, the parameter $K_u = D_d^{K^o} + D_d^{\bar{K}^o}$ has been adjusted[4] to agree with the electroproduction measurements of Cohen et al. (DECO collaboration)[16] referred to here as (Sehgal/Cornell). The normalizations used for $\int_{0.1}^{1.0} D_d^{K^o}(z)\, dz$ are equal to 0.34 (FF), 0.25 (Sehgal), and 0.20 (Sehgal/Cornell). Charmed meson production was accounted for by parameterizing non-leptonic D decay into neutral strange particles in 2-, 3-, 4-, and 5-body final states. Phase-space decay spectra were assumed using the branching fractions of Quigg and Rosner.[17] The z distributions for K_s^o originating from D mesons were obtained by convoluting the above spectra with a charm fragmentaion shape of the form z(1 − z) designed to match the z distributions measured in the $\nu Ne \rightarrow \mu^- DX$ reactions.[18] The integrals, $\int_{0.3}^{1.0} \frac{1}{N_T} \frac{dN}{dz}\, dz$, which are dominated by d, $\bar{u}$, and s quark fragmentation are 0.030 ± 0.010 and 0.059 for Sehgal/Cornell and FF, respectively. The error in the Sehgal/Cornell prediction comes from the uncertainties in the DECO results. Our data give

$$\int_{0.3}^{1.0} \frac{1}{N_T} \frac{dN}{dz}\, dz = 0.029 \pm 0.005 \quad ,$$

which does not agree with the FF model, which was constructed before the availability of inclusive K_s^o data. Other experiments have also observed a lower strange particle production rate than predicted by the FF model.[19]

IV. Conclusions

We have measured the fractional rate for producing neutral strange particles in $\bar{\nu}p$ (νp) charged-current inelastic scattering to be 0.16 ± 0.03 (0.15 ± 0.04), in agreement with results from other high energy neutrino experiments. Further, we find that the rate for the reaction $\bar{\nu}p \rightarrow \mu^+ K_s^o x$ to be $\int_{0.3}^{1.0} \frac{1}{N_T} \frac{dN}{dz}\, dz = 0.029 \pm 0.005$, which agrees with that measured in an electroproduction experiment, but is not in agreement with an early theoretical parameterization of quark fragmentation. We have also measured the rate for $K^{-}(892)$ and $\Sigma^{-}(1385)$ in $\bar{\nu}p$ scattering to be a few percent of the total inelastic rate.

This work was supported in part by the U. S. Department of Energy and made possible through the cooperation of the Neutrino Department at Fermilab. We gratefully acknowledge the years of service given to each of the three institutions by their individual scanning staffs in the final phases of a long bubble chamber program. We are indebted to Prof. Lincoln Wolfenstein of CMU and Prof. John Donoghue of the University of Massachusetts for many useful conversations.

Appendix

Monte Carlo Analysis

In order to simulate the production of neutral strange particles, the MC program, described in Ref. 3, was modified slightly. The event generation scheme was retained except that for each generated event, two extra neutral tracks were created. The momenta of these tracks were then assigned in the same manner as those of the non-strange tracks except that the values of these momenta were chosen from the shapes derived from the observed longitudinal and transverse momenta of the K_s^o and Λ tracks. The K_s^o and Λ masses were randomly assigned to those tracks in the ratio 2:1 as found in the experiment.

Three mechanisms are responsible for the production of strange particles: Cabibbo production by antineutrinos, charm production, and associated production. The first mechanism is a minor source of strange particles and is ignored. Because associated production forms the bulk of strange particle production, we assumed, for the purpose of improving the energy determination, that all of the strange particle production is from this source. We assigned the visibility of strange particles according to the probabilities of their materialization. Most resulting final states have one strange track "visible" and one "invisible".

Figure 19 shows the momentum distribution of the K_s^o and Λ from the charged current events observed in the experiment. The curve which represents the data is the input to the MC program. Figure 20 shows the P_L-P_T correlation for the hadronic system from these strange particle events. The data points are those of Fig. 4, and the straight line is that generated by the MC program.

Using the energy determination method described in the text, we show in Fig. 21 the x and y distributions for the normalized MC $\bar{C}C$ events in the solid curves. The curves follow the observed strange particle data shown in the histograms. The dashed lines show the x and y distributions for the inclusive sample. Because we are generating events as associated production pairs, we expect the x distribution for the MC events to be similar to the inclusive data. As is seen, kinematic restrictions cause the MC strange particle events to have a small distortion at low y from the dominant $(1-y)^2$ shape of the strange particle data. Because we have not modeled charm production, the strange particle data should tend more toward lower x and higher y values than either the MC events or the inclusive data.

Figure 22 shows the resolutions in E_ν, E_{HAD}, x, and y for $\bar{C}C$ events generated in the MC program and selected by the criteria described in Section II. Also shown as dashed lines are the same resolutions for inclusive $\bar{C}C$ events from the unmodified MC program. Clearly, with the modifications described above, events with strange particles have resolutions comparable to the non-strange events.

References

a) Present Address: Fermi National Accelerator Laboratory, Batavia, IL 60510.

b) Present Address: U.S. Department of Energy, Washington, D.C. 20545.

c) Present Address: University of Toronto, Toronto, Ont., Canada.

d) Present Address: Lawrence Livermore Laboratory, Livermore, CA 94550.

e) Present Address: CERN, EP Divsion, Geneva 2?, Switzerland.

f) Present Address: Bell Telephone Laboratories, Naperville, IL 60540.

g) Present Address: Argonne National Laboratory, Argonne, IL 60439.

1. S. J. Barish et al., Phys. Rev. Letters 45, 783 (1980).

2. We use the standard variables: E_ν, the neutrino energy; M_p, the proton mass; W, the invariant hadronic mass, Q^2, the negative of the four-momentum transfer squared; $\nu = E_\nu - E_\mu$, where E_μ is the muon energy; $x = Q^2/2M_p\nu$, and $y = \nu/E_\nu$. The Feynman x variable is defined as $x_F = 2P_L^*/W$, with P_L^* defined as the momentum component in the hadronic CM system along the direction of the momentum transfer.

3. V. E. Barnes et al., "Measurement of the Quark Momentum Distributions in the Proton Using an Antineutrino Probe", Purdue COO-1428-480, submitted to Phys. Rev.

4. In part, these indicators included: A minimum chi-squared probability cut of 10^{-4} applied to each fit; a comparison and cut on the ratio of positive-to-negative track momenta; and a cut on the "momentum" assigned to the recoil, impulse proton track of the γ hypothesis by the program SQUAW. Further details can be found in R. Brock, Ph.D. Thesis,

Carnegie-Mellon University (1980), unpublished.

5. M. Derrick et al., Phys. Rev. D18, 7 (1978).

6. V. V. Ammosov et al., Nucl. Phys. B162, 205 (1980).

7. J. P. Berge et al., Phys. Rev. D18, 1359 (1978).

8. H. Grässler et al., CERN/EP 81-56, submitted to Nucl. Phys. B.

9. F. A. Nezrick, SLAC Summer Institute talk (1976) (unpublished).

10. J. P. Berge et al., Phys. Rev. Letters 36, 127 (1976).

11. J. Ballam et al., Phys. Rev. Letters 56B, 193 (1975).

12. A. J. Sadoff et al., Phys. Rev. Letters 32, 955 (1974) and H. H. Bingham et al., Phys. Rev. D8, 127 (1973).

13. M. Derrick et al., Phys. Rev. D24, (1981).

14. R. D. Field and R. P. Feynman, Phys. Rev. D15, 2590 (1977).

15. L. M. Sehgal in Proceedings of the 1977 International Symposium on Lepton and Photon Interactions at High Energies, Ed. Hamburg (1977).

16. I. Cohen et al., Phys. Rev. Letters 40, 1614 (1978).

17. C. Quigg and J. L. Rosner, Phys. Rev. D16, 1497 (1977).

18. C. Baltay, Phys. Rev. Letters 41, 73 (1978).

19. V. V. Ammosov et al., Phys. Letters 93, 210 (1980).

Table I. Scanning efficiency and pass rates as a function of charged multiplicity for both the inclusive sample and the events with a neutral decay.

	Inclusive Sample		V^o Sample
# Charged Tracks	Scanning Efficiency	Pass Rate	Scanning Efficiency for Find'ng V^o
3	0.79 ± 0.04	0.93 ± 0.02	0.98 ± 0.02
5	0.92 ± 0.04	0.94 ± 0.02	0.97 ± 0.02
7	0.93 ± 0.03	0.84 ± 0.03	1.00 ± 0.02
9	0.98 ± 0.02	0.80 ± 0.05	0.98 ± 0.02
≥ 11	1.00 ± 0.02	0.74 ± 0.05	0.98 ± 0.02

Table II. Classification of all V's, G's, and A's.

Original Classification	Number of Events	Final Event Numbers		
		K	Λ	γ
K	139	139		
Λ	86		86	
γ	638			638
K, Λ	15	3	12	
K, γ	71	66		5
Λ, γ	50		25	25
K, Λ, γ	25	6	12	7
	Totals:	214	135	675

Table III. Event classifications for final states containing a strange particle.

Observed Reaction	Observed No. of Events	Final State	Corrected No. of Events	Fractional Rate
$\bar{\nu}p \to \mu^+ K^o_s X^o$	78	$\mu^+ K^o X^o$	258 ± 67[a]	0.095 ± 0.024
$\bar{\nu}p \to \mu^+ \Lambda^o X^o$	40	$\mu^+ \Lambda(\Sigma^o) X^o$	80 ± 19[b]	0.029 ± 0.007
$\bar{\nu}p \to \mu^+ \Lambda^o K^o_s X^o$	6	$\mu^+ \Lambda(\Sigma^o) K^o X^o$	45 ± 14	0.016 ± 0.005
$\bar{\nu}p \to \mu^+ K^o_s K^o_s X^o$	2	$\mu^+ K^o \bar{K}^o X^o$	63 ± 36	0.02 ± 0.01
Total	126		446 ± 80	0.16 ± 0.03

Observed Reaction	Observed No. of Events	Final State	Corrected No. of Events	Fractional Rate
$\nu p \to \mu^- K^o_s X^{++}$	21	$\mu^- K^o X^{++}$	90 ± 21[a]	0.12 ± 0.03
$\nu p \to \mu^- \Lambda^o X^{++}$	4	$\mu^- \Lambda(\Sigma^o) X^{++}$	0 ± 12[b]	
$\nu p \to \mu^- \Lambda K_s X^{++}$	2	$\mu^- \Lambda(\Sigma^o) K^o X^{++}$	23 ± 16	0.03 ± 0.02
$\nu p \to \mu^- K^o_s K^o_s X^{++}$	0	$\mu^- K^o \bar{K}^o X^{++}$	0	
Total	27		113 ± 29	0.15 ± 0.04

[a] The corrected numbers given are for the final states where X^o does not contain a $\Lambda(\Sigma^o)$ or K^o.

[b] The corrected numbers given are for the final states where X^o does not contain a K^o.

Table IV. Relative strange particle production for high energy neutrino (R_ν) and antineutrino ($R_{\bar{\nu}}$) scattering from this and other experiments.

Reference	Reaction	R_ν	$R_{\bar{\nu}}$
This experiment	$\bar{\nu}p$		0.16 ± 0.03
6	$\bar{\nu}Ne$		0.16 ± 0.03
This experiment	νp	0.15 ± 0.04	
7	νp	0.14 ± 0.02	
8	νp	0.174 ± 0.008	

Figure Captions

Fig. 1 Calculated shape of the wide-band antineutrino flux together with the background neutrino flux (see Ref. 3).

Fig. 2 Median P_L-P_T correlation for the charged hadronic systems in $\bar{\nu}p$ $\overline{CC}$ events. The straight lines show the $\langle P_L \rangle : P_T$ correlation used in this experiment to determine the neutrino energy for events without visible strange particles. The error bars represent the RMS spread of P_L for a fixed interval of P_T.

Fig. 3 Momentum vectors for a $\bar{\nu}p$ CC event. $\vec{P}_\nu$ and $\vec{P}_\mu$ refer to the antineutrino and muon momenta, while $\vec{H}^o$ and $\vec{H}^c$ refer to the total vector momenta of the neutral and charged outgoing hadrons.

Fig. 4 Mean P_L-P_T correlation for the hadronic system, including the observed neutral strange particles in $\overline{CC}$ and CC events containing a visible strange particle decay. The solid straight line is a fit to these data. The dashed lines are the fits to the charged hadronic system shown in Fig. 2. The error bars represent the RMS spread of P_L for a fixed interval of P_T.

Fig. 5 Corrected neutrino energy distributions for events with strange particles for (a) $\overline{CC}$ and (b) CC events. The curves are the corresponding inclusive distributions.

Fig. 6 Corrected distributions in energy transfer ν for events with strange particles for (a) $\overline{CC}$ and (b) CC events. The curves are the corresponding inclusive distributions.

Fig. 7 Corrected x distributions for events with strange particles for (a) $\overline{CC}$ and (b) CC events. The curves are the corresponding inclusive distributions.

Fig. 8 Corrected y distributions for events with strange particles for (a) $\bar{C}\bar{C}$ and (b) CC events. The curves are the corresponding inclusive distributions.

Fig. 9 Corrected W distributions for events with strange particles for (a) $\bar{C}\bar{C}$ and (b) CC events. The curves are the corresponding inclusive distributions.

Fig. 10 Corrected Q^2 distributions for events with strange particles for (a) $\bar{C}\bar{C}$ and (b) CC events. The curves are the corresponding inclusive distributions.

Fig. 11 Visible V^o fraction versus W for various lepton- and photon-induced processes: $\bar{\nu}p$, νp this experiment; $\bar{\nu}N$, Ref. 9; νp, Ref. 6; electro- and muo-production, Ref. 11; and photoproduction, Ref. 12.

Fig. 12 Corrected invariant $\Lambda\pi^+$ mass distributions for (a) $\bar{C}\bar{C}$ and (b) CC events.

Fig. 13 Corrected invariant $\Lambda\pi^-$ mass distributions for (a) $\bar{C}\bar{C}$ and (b) CC events.

Fig. 14 Corrected invariant $K^o_s\pi^+$ mass distributions for (a) $\bar{C}\bar{C}$ and (b) CC events.

Fig. 15 Corrected invariant $K^o_s\pi^-$ mass distributions for (a) $\bar{C}\bar{C}$ and (b) CC events. The curve in (a) is the normalized $\bar{C}\bar{C}$ $K^o_s\pi^+$ distribution.

Fig. 16 Corrected $K^o_s\pi^+\pi^-$ invariant mass combinations in $\bar{C}\bar{C}$ events.

Fig. 17 (a) The z distribution for corrected $\bar{C}\bar{C}$ production of K^o_s. The solid curve is the flux-integrated Sehgal/Cornell parameterization, including charm production for $x > 0.05$ and $0.1 < y < 0.8$. The dashed curve is the same quantity for the FF prediction in the same (x,y) region. (b) The z distribution for corrected CC production of K_s^o.

Fig. 18 The z distribution for fully corrected Λ production in (a) $\overline{CC}$ events, and (b) CC events.

Fig. 19 Strange particle momentum distributions for the CC and $\overline{CC}$ event sample. The curve is the input to the MC calculation.

Fig. 20 P_L-P_T correlation for strange particle events from the MC (line) and the data from Fig. 4.

Fig. 21 The histogram shows the x and y distributions for the strange particle $\overline{CC}$ sample. The solid curve is the MC prediction, and the dashed curve shows the shape of the inclusive $\overline{CC}$ sample.

Fig. 22 The MC predictions for the resolutions of different kinematic quantities for the $\overline{CC}$ events with visible strange particles (full histogram) and for the inclusive sample (dashed histogram): a) $\Delta E/E$, b) $\Delta E_{HAD}/E_{HAD}$, c) Δx, and d) Δy.

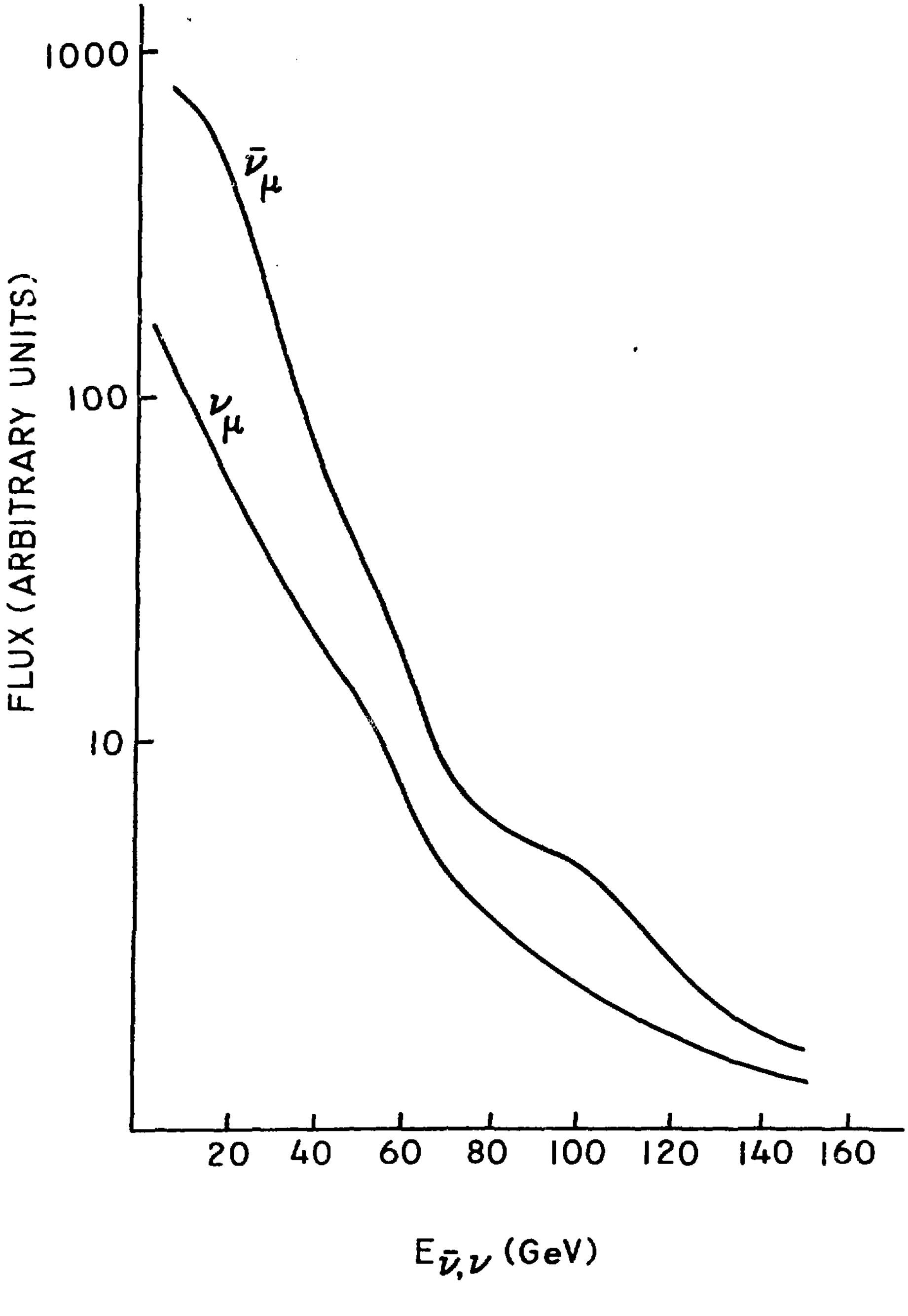

FLUX (ARBITRARY UNITS)
1000
100
10
$\bar{\nu}_\mu$
ν_μ
20
40
60
80
100
120
140
160
$E_{\bar{\nu},\nu}$ (GeV)

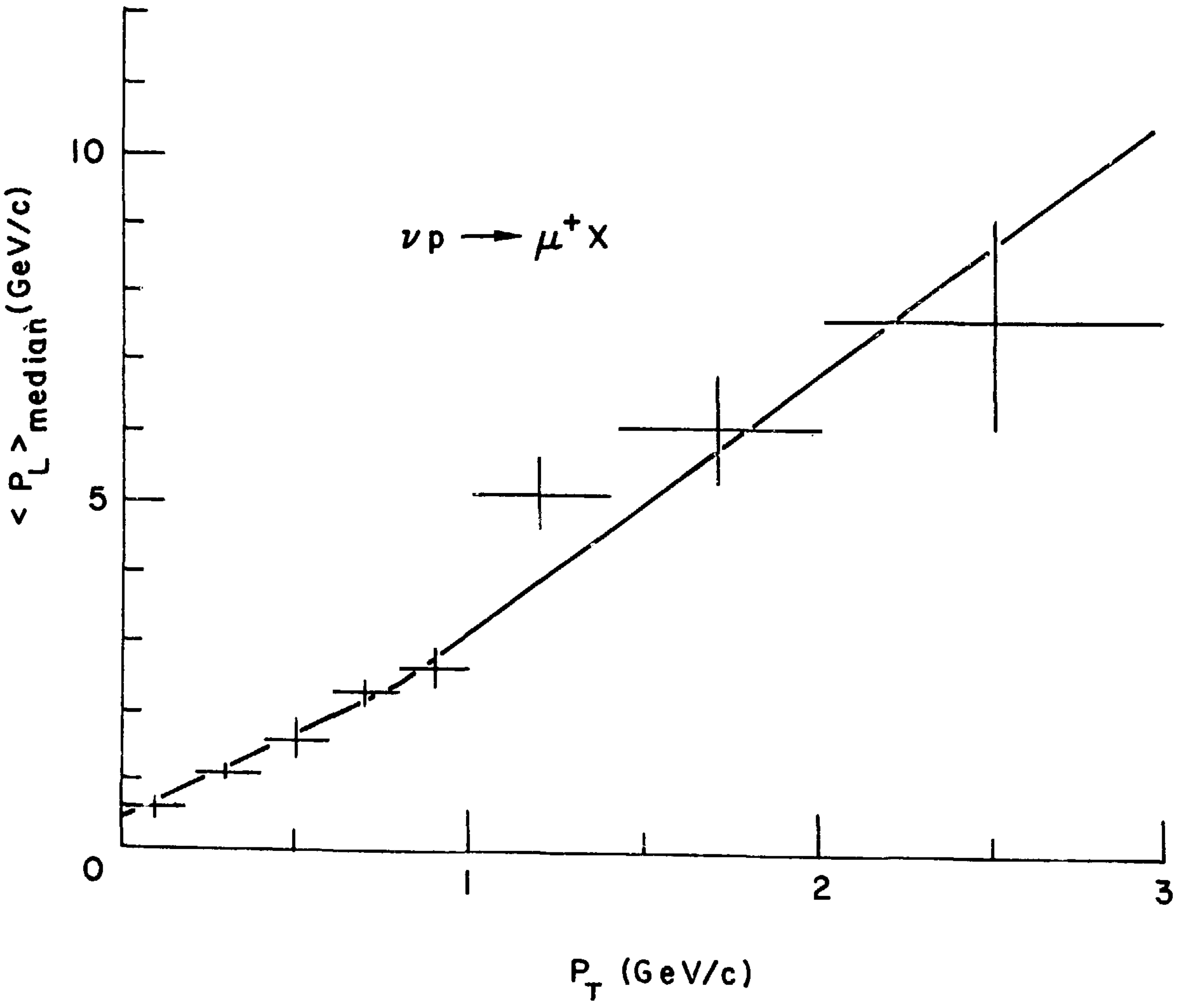

10
5
0
1
2
3
$\langle P_L \rangle_{median}$ (GeV/c)
$\nu p \rightarrow \mu^+ X$
P_T (GeV/c)

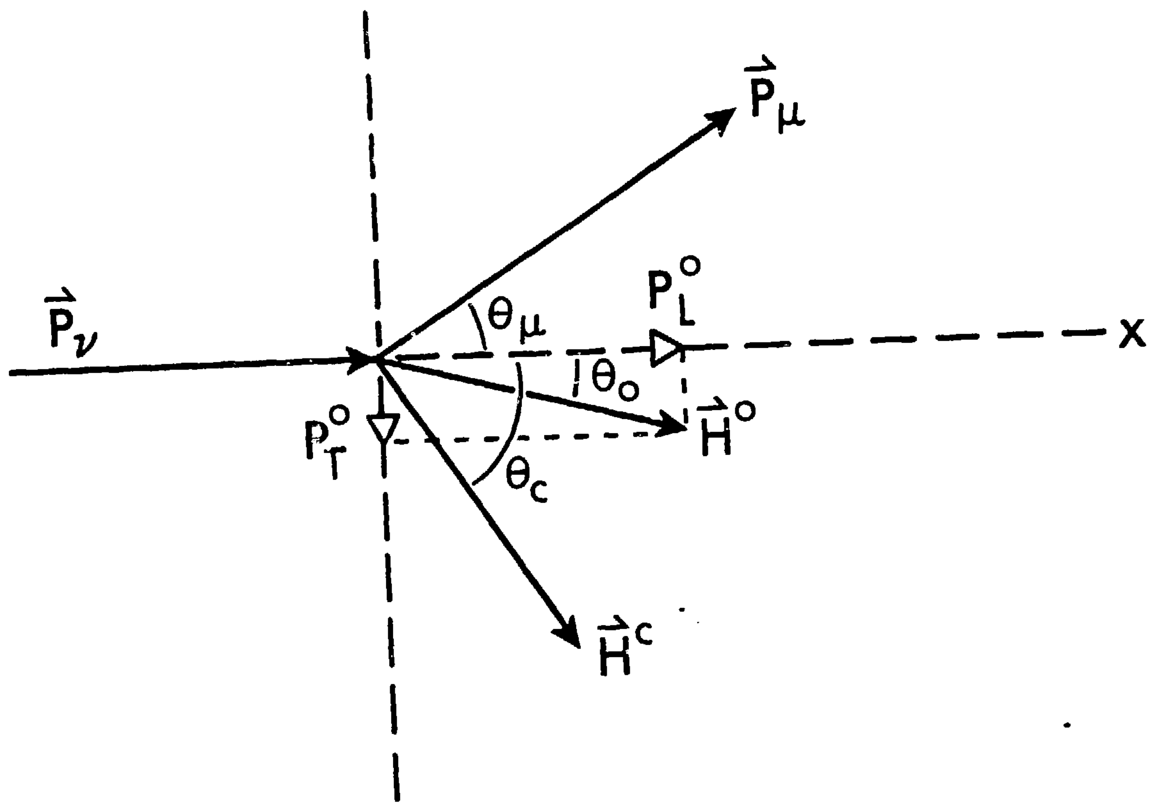

$\vec{P}_\mu$
P_L^o
X
$\vec{P}_\nu$
θ_μ
θ_o
$\vec{H}^o$
P_T^o
θ_c
$\vec{H}^c$

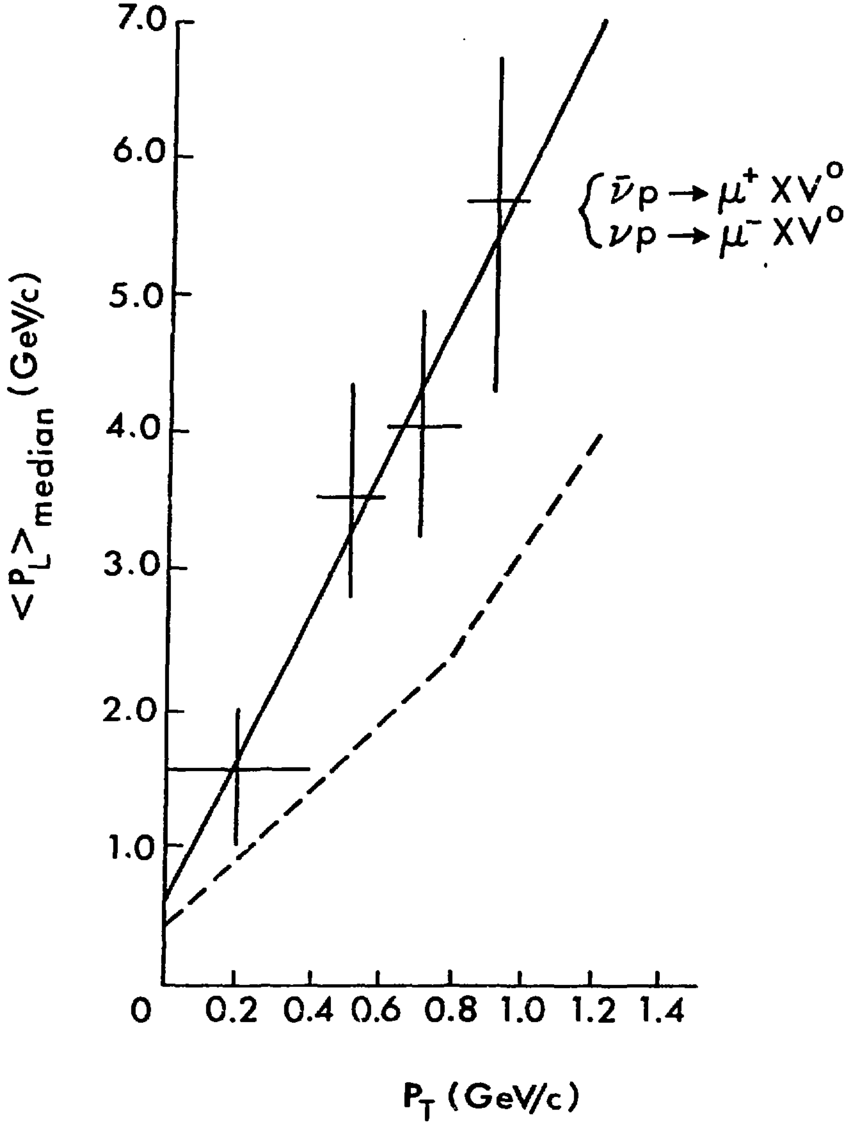

7.0
6.0
5.0
4.0
3.0
2.0
1.0
0
0.2
0.4
0.6
0.8
1.0
1.2
1.4
$\langle P_L \rangle_{median}$ (GeV/c)
P_T (GeV/c)
$\bar{\nu} p \to \mu^+ X V^o$
$\nu p \to \mu^- X V^o$

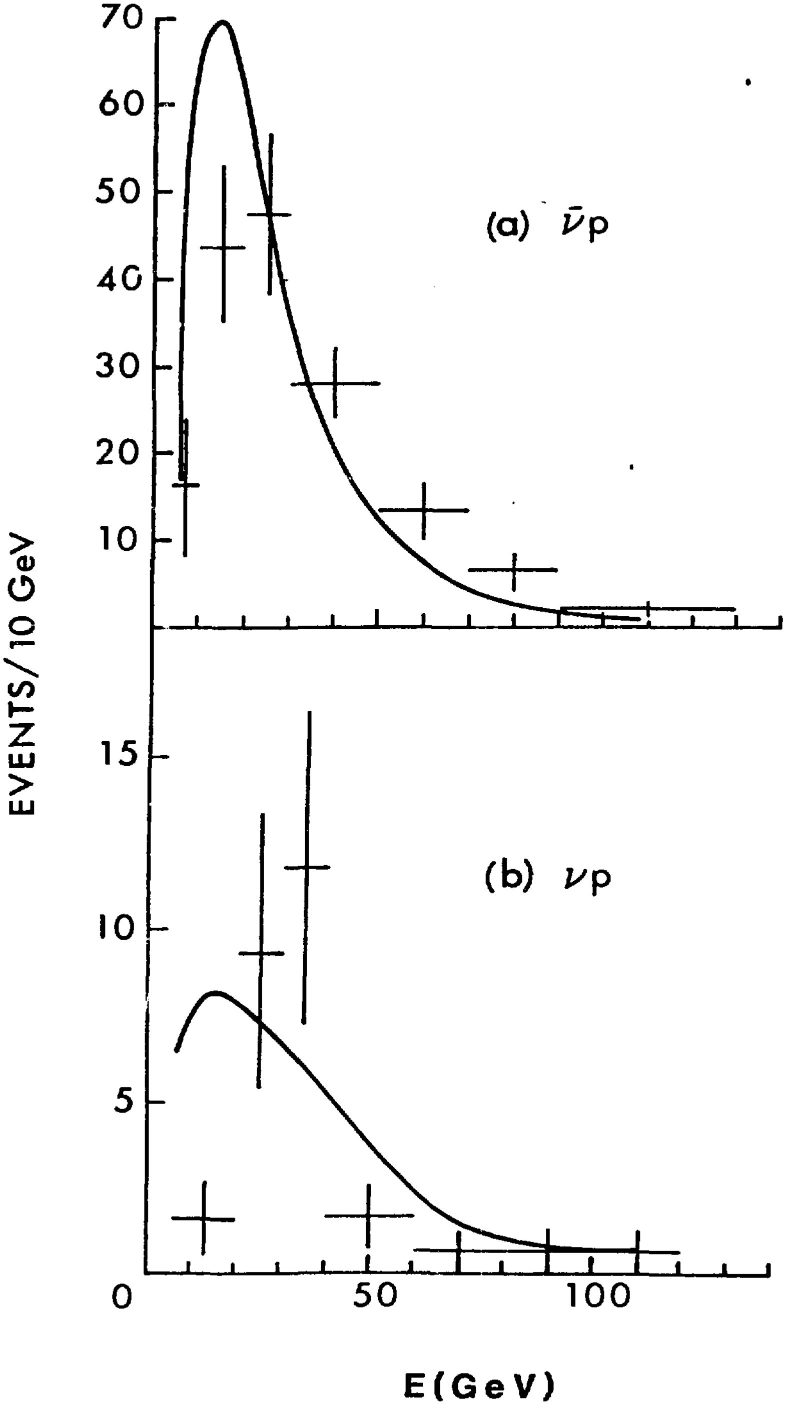
70
60
50
40
30
20
10
(a) $\bar{\nu}$p
EVENTS/10 GeV
15
10
5
0
(b) νp
50
100
E(GeV)

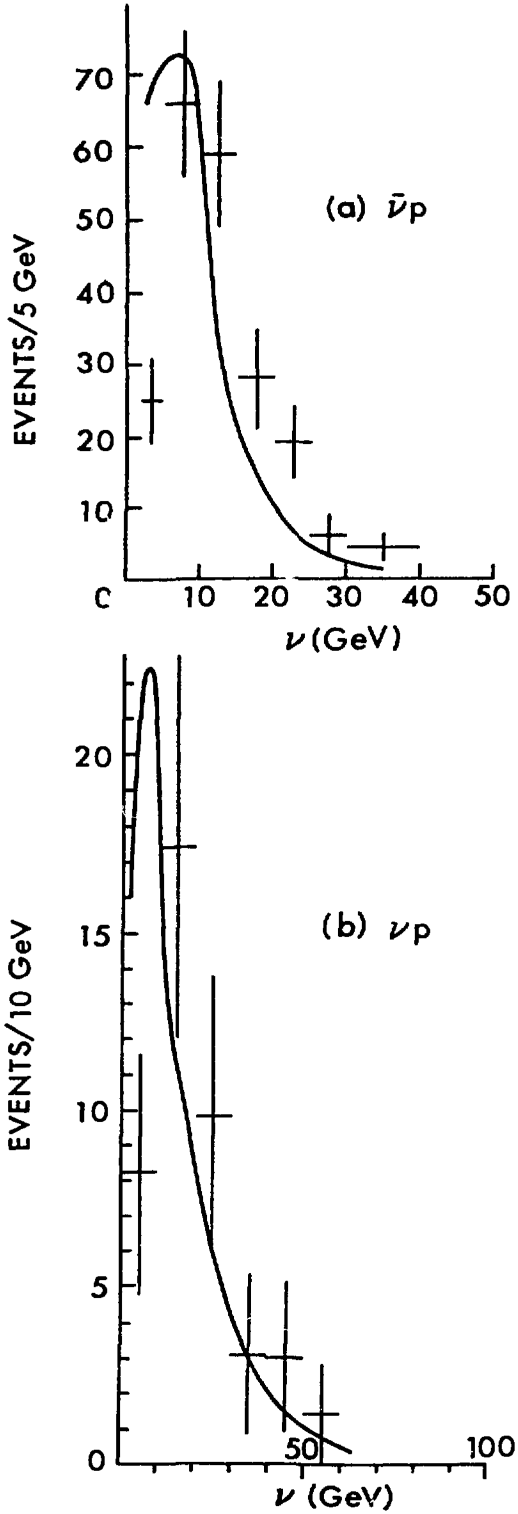

EVENTS/5 GeV
70
60
50
40
30
20
10
C
10
20
30
40
50
ν (GeV)
(a) ν̄p
EVENTS/10 GeV
20
15
10
5
0
50
100
ν (GeV)
(b) νp

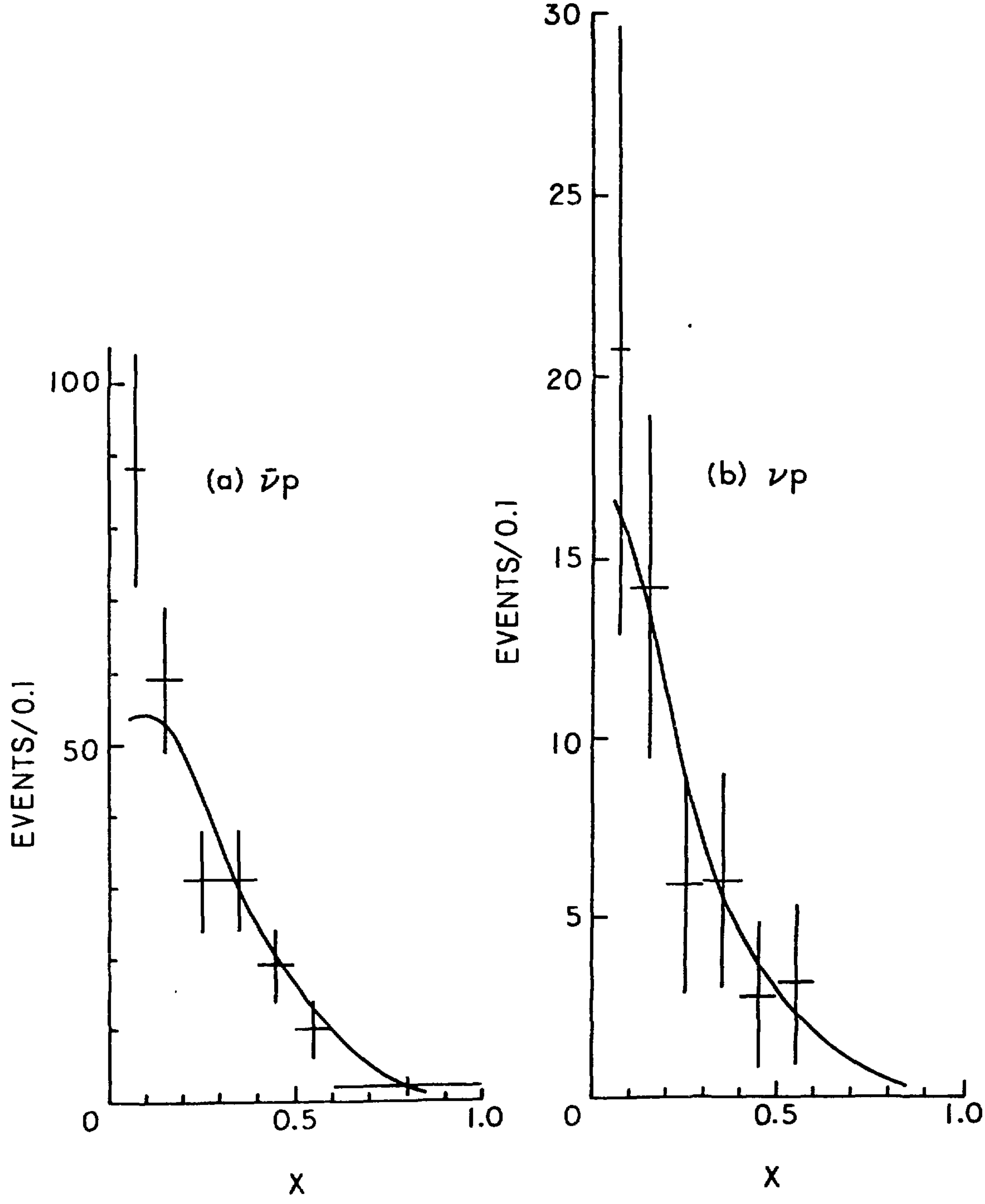

(a) ν̄p
EVENTS/0.1
100
50
0
0.5
1.0
X
(b) νp
EVENTS/0.1
30
25
20
15
10
5
0
0.5
1.0
X

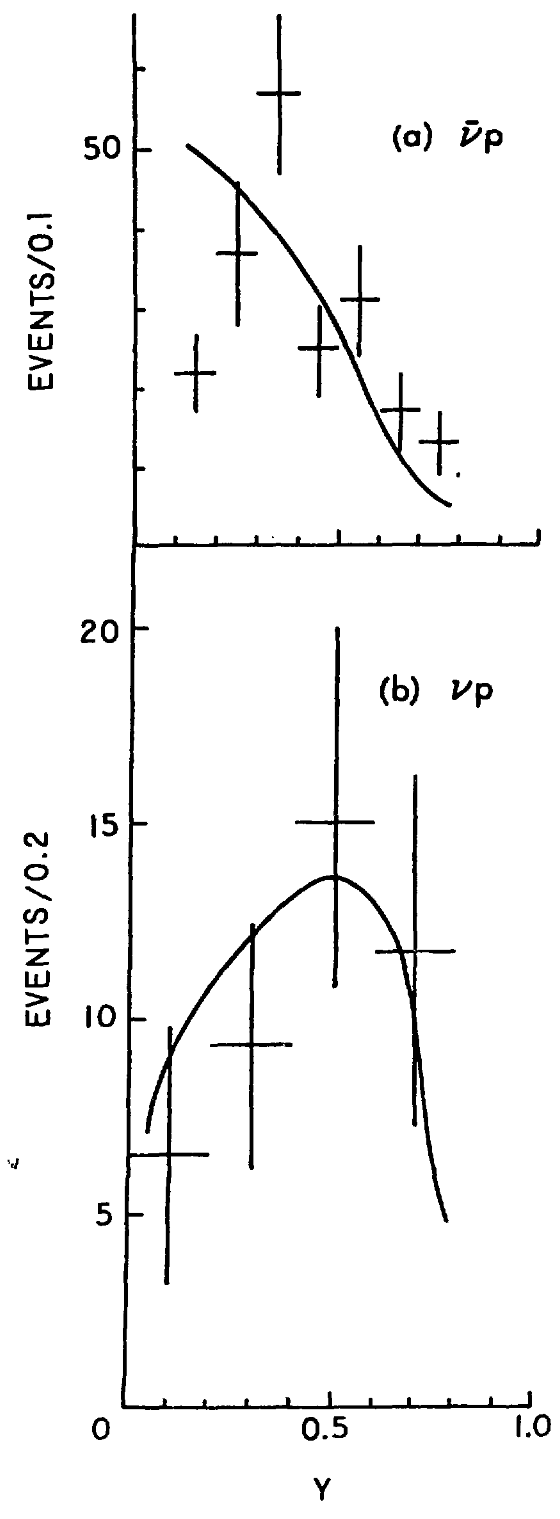
(a) $\bar{\nu}p$
EVENTS/0.1
50
(b) νp
EVENTS/0.2
20
15
10
5
0
0.5
1.0
Y

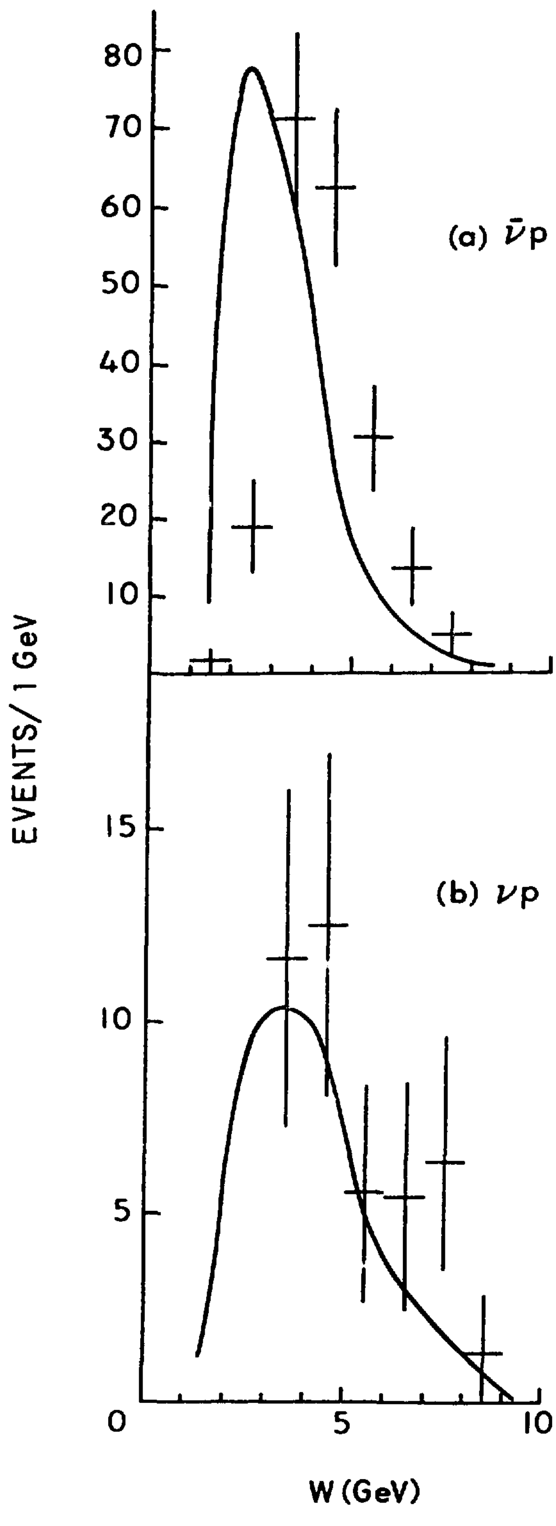

80
70
60
50
40
30
20
10
(a) $\bar{\nu}$p
EVENTS/ 1 GeV
15
10
5
(b) νp
0
5
10
W (GeV)

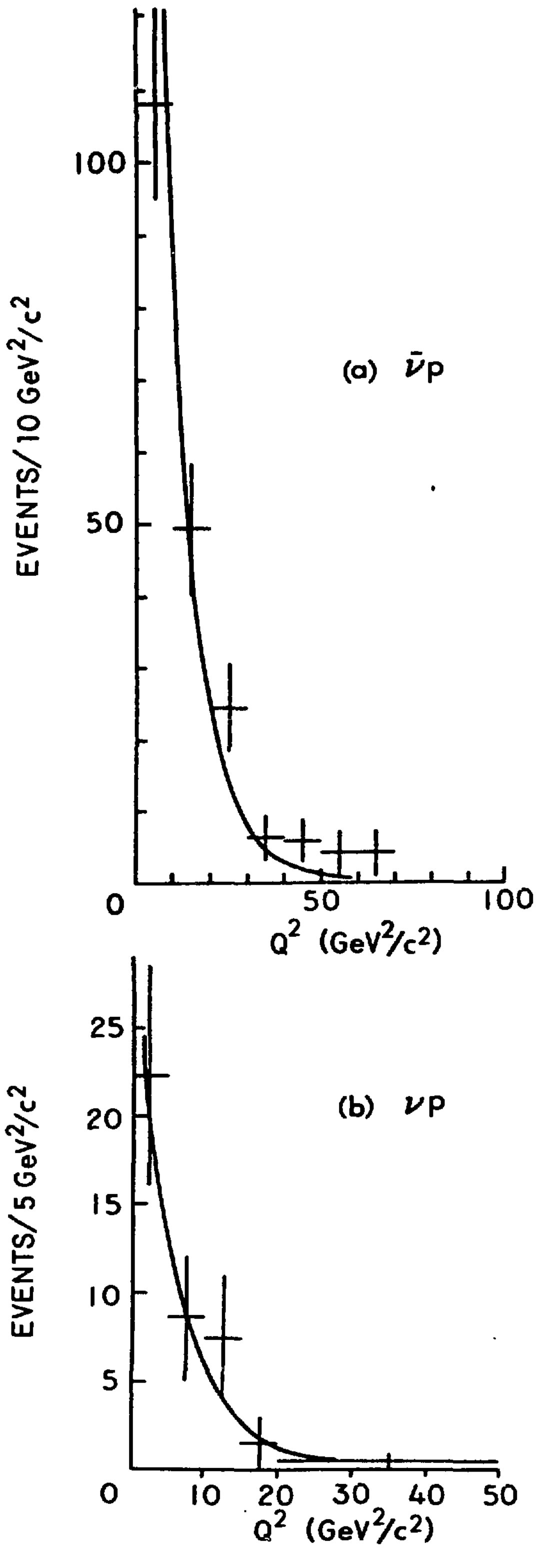
EVENTS/10 GeV^2/c^2
(a) $\bar{\nu}$p
0
50
100
Q^2 (GeV^2/c^2)
EVENTS/5 GeV^2/c^2
(b) νp
0
5
10
15
20
25
30
40
50
Q^2 (GeV^2/c^2)

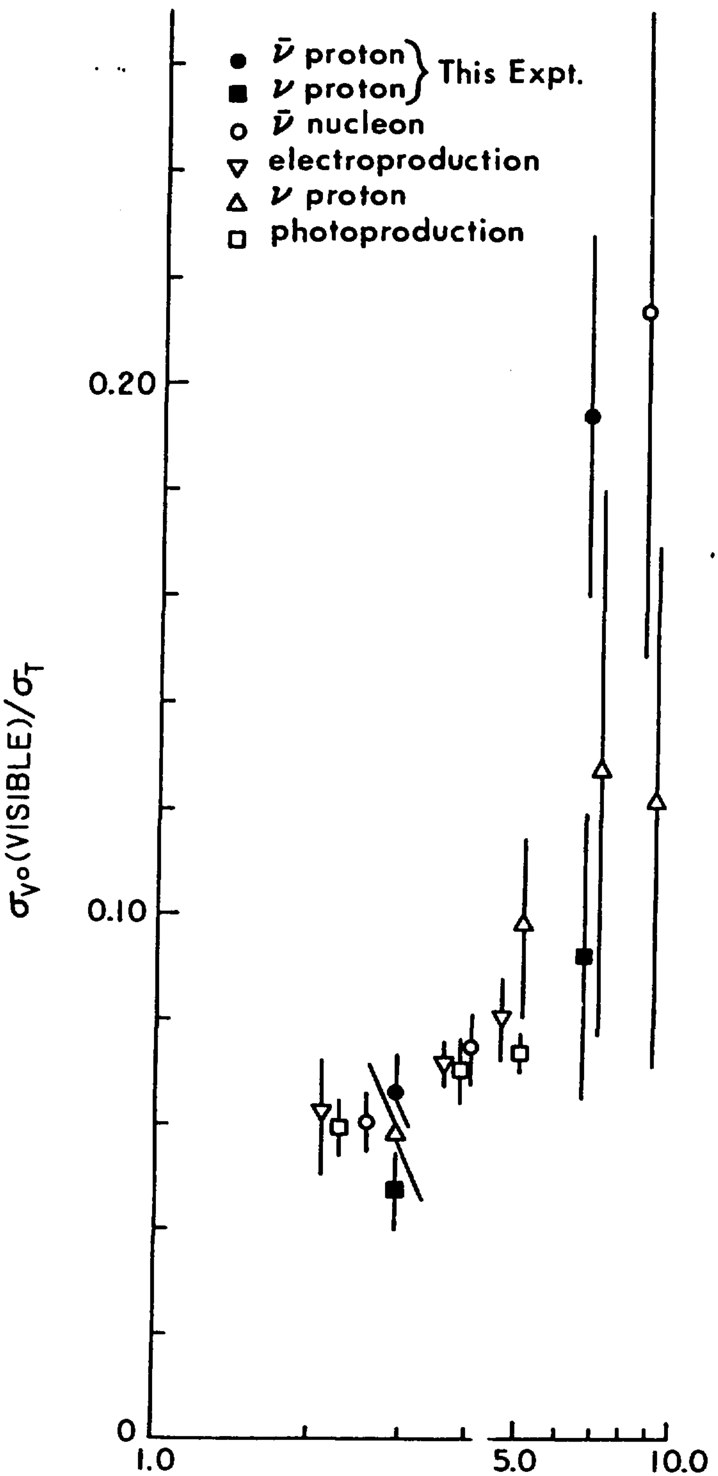

$\bar{\nu}$ proton
ν proton
This Expt.
$\bar{\nu}$ nucleon
electroproduction
ν proton
photoproduction
0.20
0.10
0
1.0
5.0
10.0
W (GeV)
σ_{V^0}(VISIBLE)/σ_T

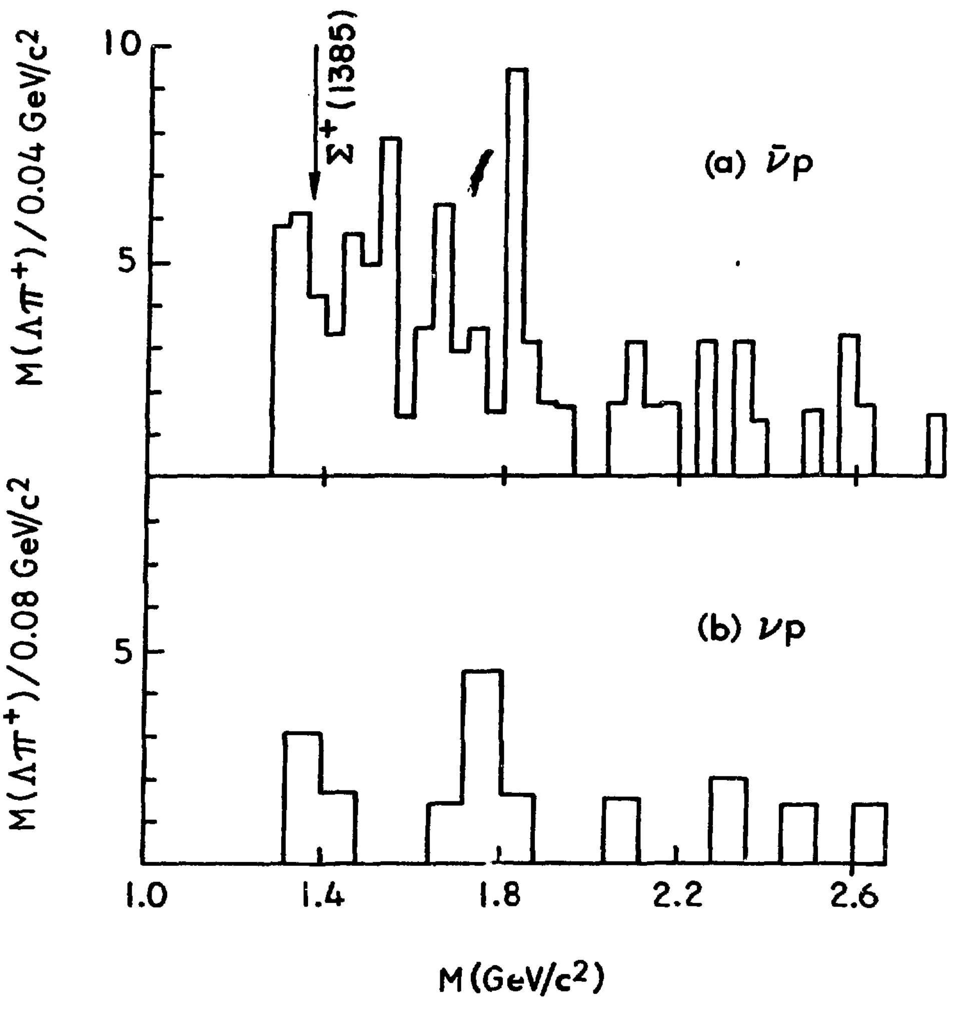

M(Λπ⁺)/0.04 GeV/c²
10
5
Σ⁺(1385)
(a) ν̄p
M(Λπ⁺)/0.08 GeV/c²
5
(b) νp
1.0
1.4
1.8
2.2
2.6
M(GeV/c²)

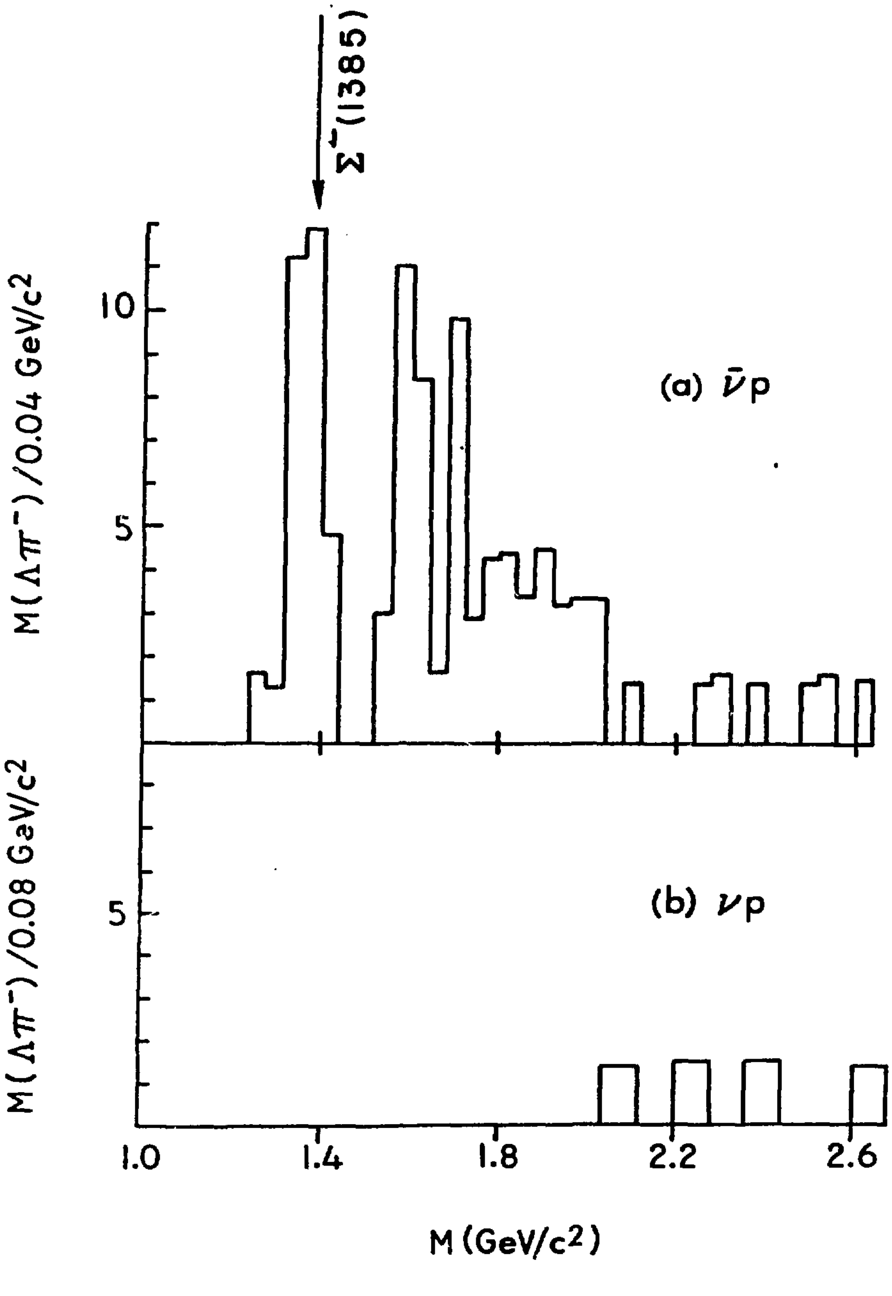

$\Sigma^{*-}(1385)$
10
5
(a) $\bar{\nu}$p
M($\Lambda\pi^-$) /0.04 GeV/c^2
5
(b) νp
M($\Lambda\pi^-$) /0.08 GeV/c^2
1.0
1.4
1.8
2.2
2.6
M (GeV/c^2)

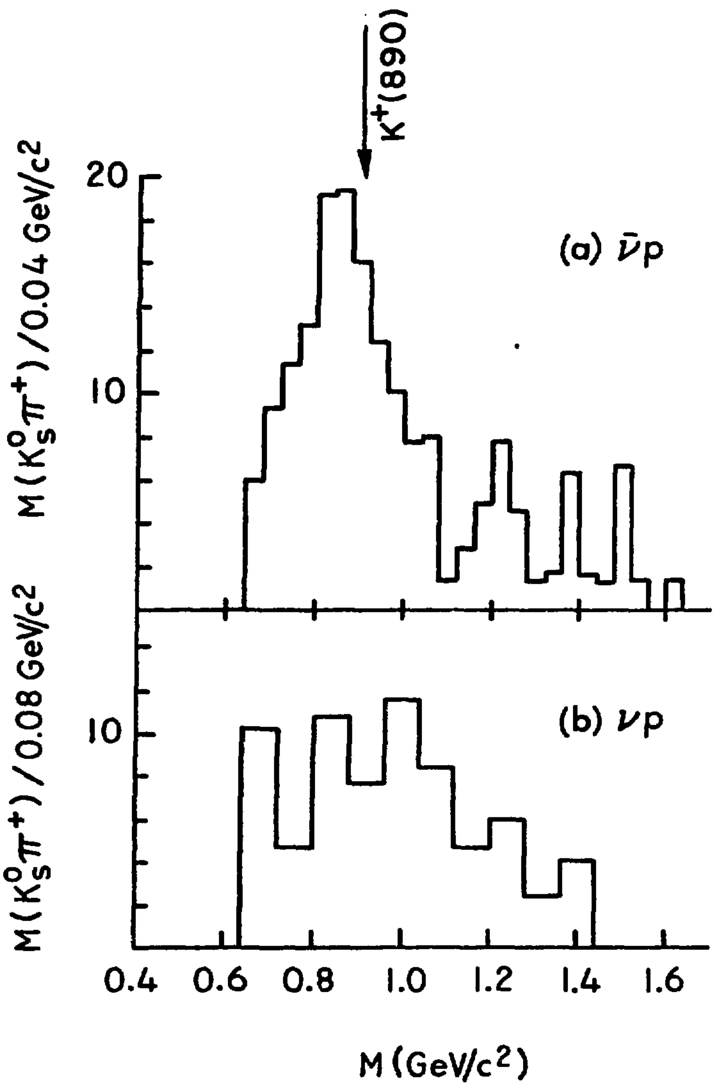

K*+(890)
20
10
M(K$^0_s\pi^+$)/0.04 GeV/c^2
(a) $\bar{\nu}$p
10
M(K$^0_s\pi^+$)/0.08 GeV/c^2
(b) νp
0.4
0.6
0.8
1.0
1.2
1.4
1.6
M (GeV/c^2)

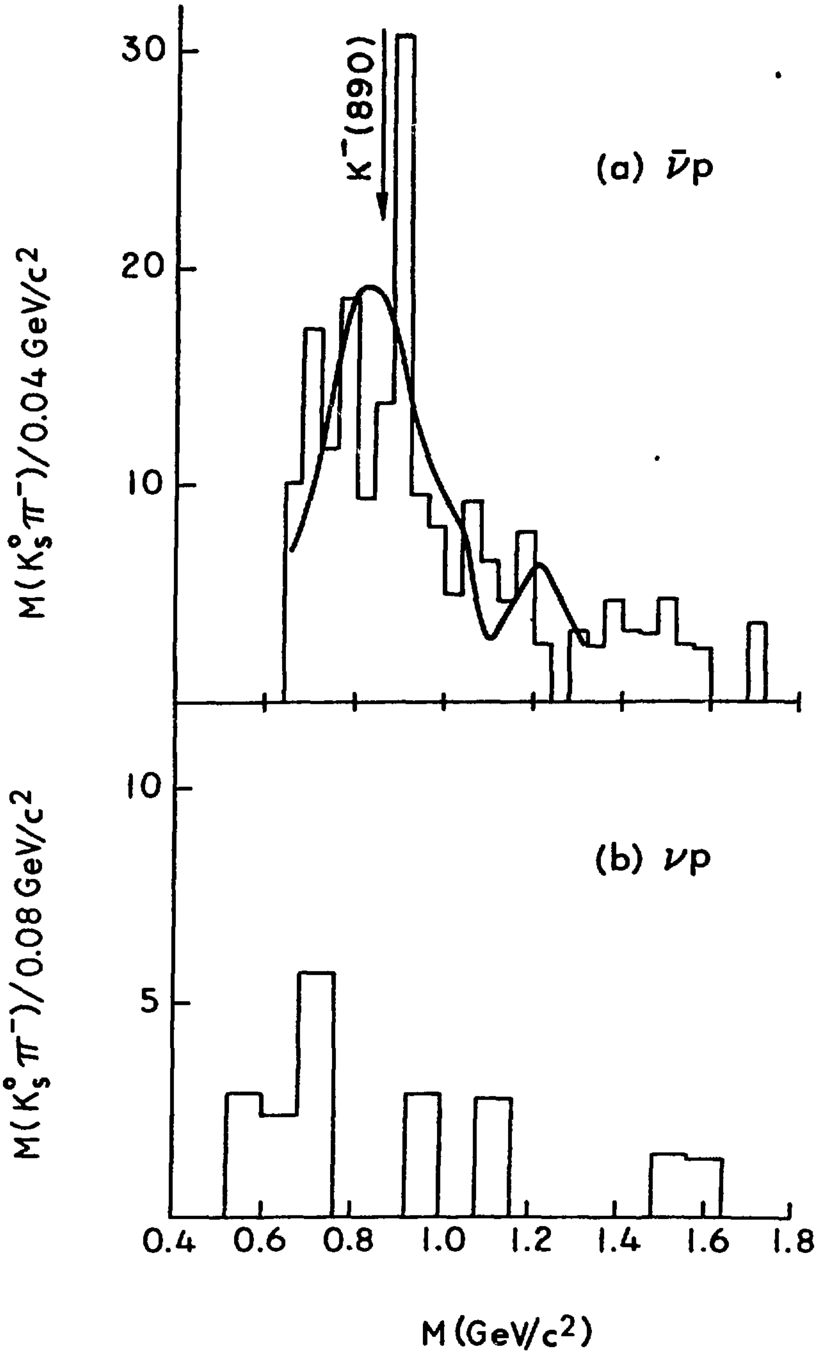

K⁻(890)
(a) ν̄p
(b) νp
M(K°s π⁻)/0.04 GeV/c²
M(K°s π⁻)/0.08 GeV/c²
30
20
10
5
0.4
0.6
0.8
1.0
1.2
1.4
1.6
1.8
M (GeV/c²)

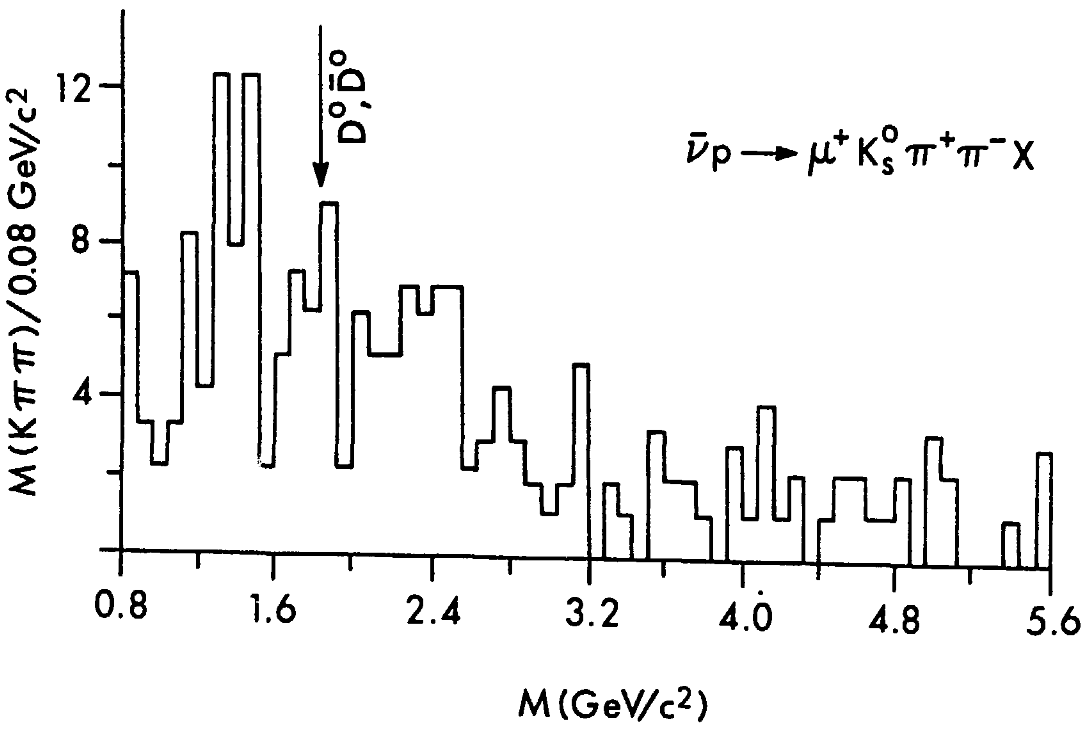

M(Kππ)/0.08 GeV/c²
12
8
4
D⁰,D̄⁰
ν̄p → μ⁺ K⁰s π⁺π⁻ X
0.8
1.6
2.4
3.2
4.0
4.8
5.6
M(GeV/c²)

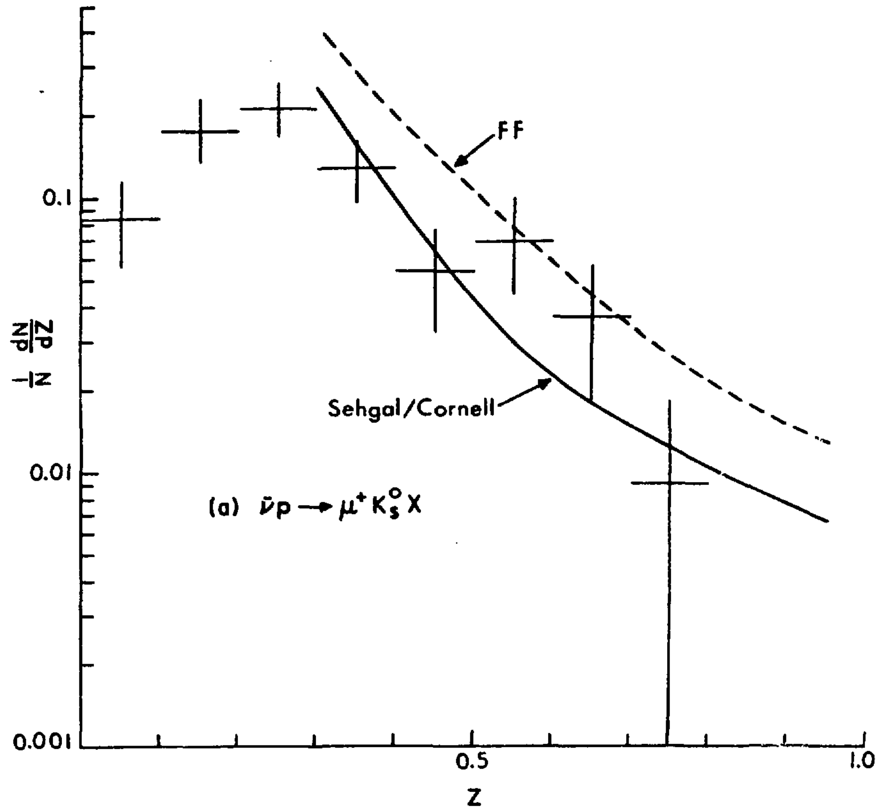
FF
Sehgal/Cornell
0.1
0.01
0.001
(a) $\bar{\nu}p \rightarrow \mu^+ K_s^0 X$
$\frac{1}{N}\frac{dN}{dZ}$
0.5
1.0
Z

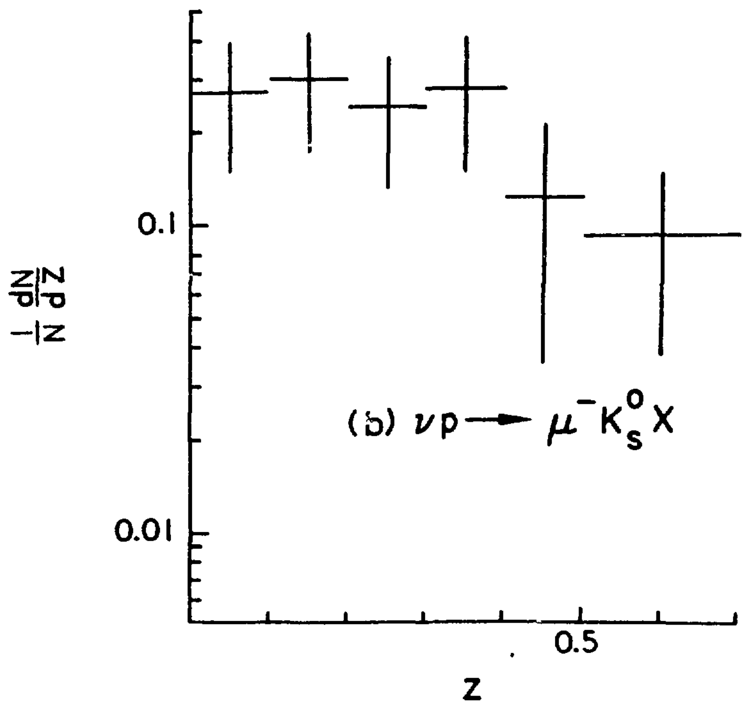
0.1
0.01
$\frac{1}{N}\frac{dN}{dZ}$
(b) $\nu p \rightarrow \mu^- K_s^0 X$
0.5
Z

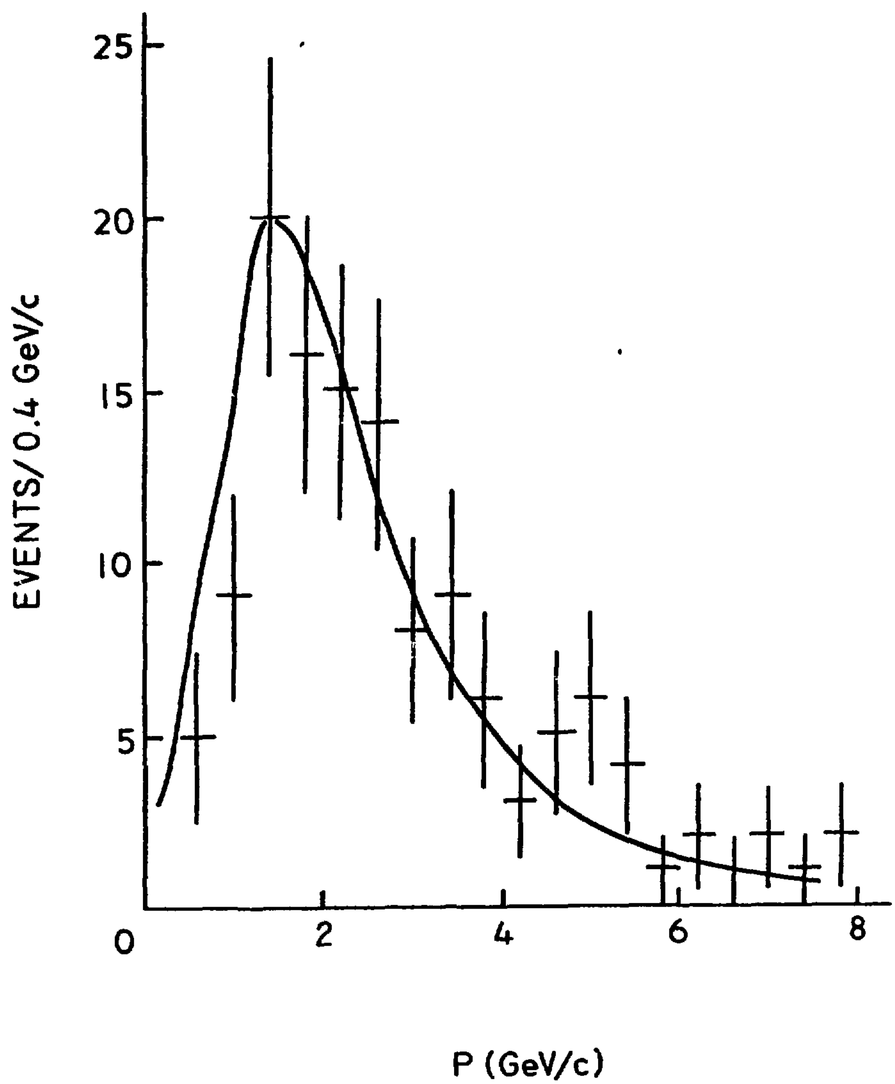
EVENTS/ 0.4 GeV/c
25
20
15
10
5
0
2
4
6
8
P (GeV/c)

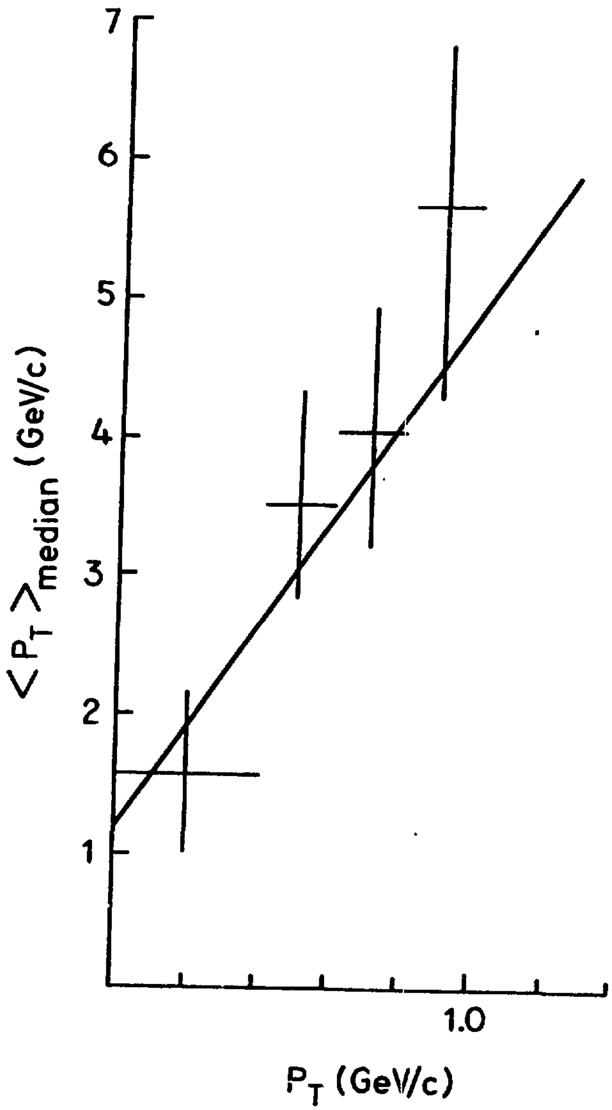

7
6
5
4
3
2
1
$\langle P_T \rangle_{median}$ (GeV/c)
1.0
P_T (GeV/c)

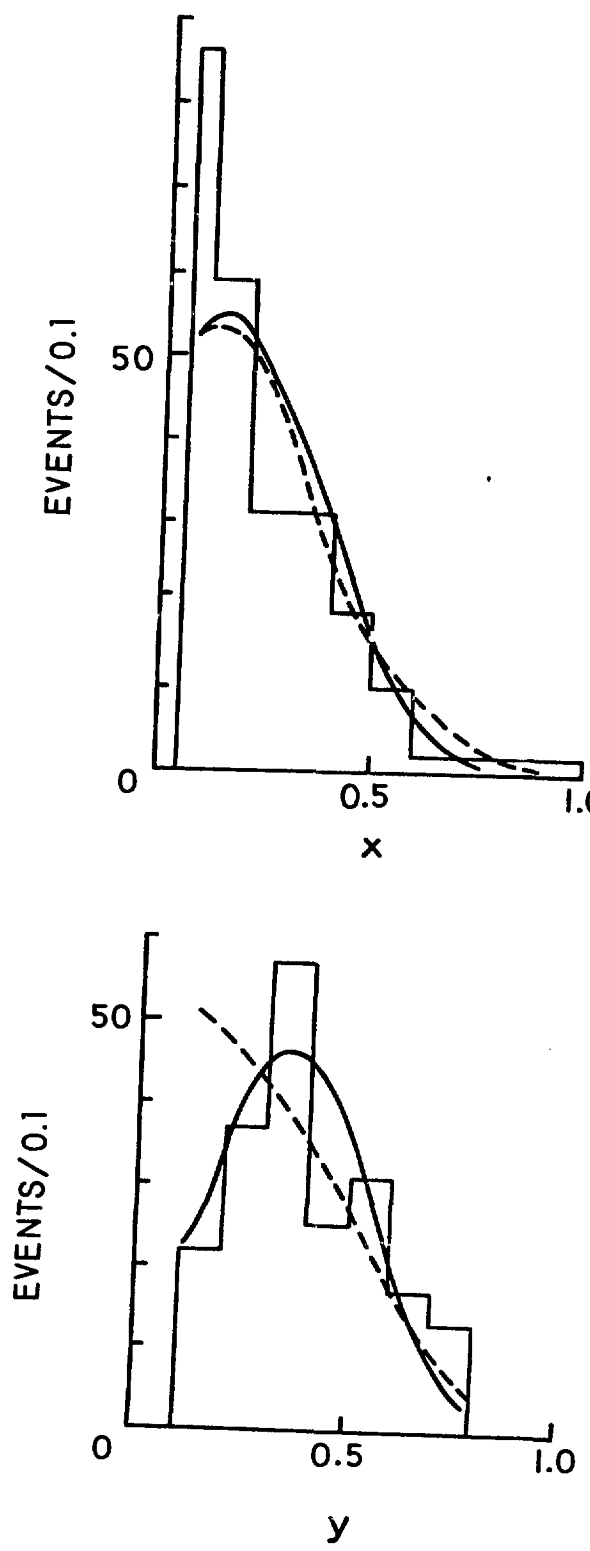
EVENTS/0.1
50
0
0.5
1.0
x
EVENTS/0.1
50
0
0.5
1.0
y

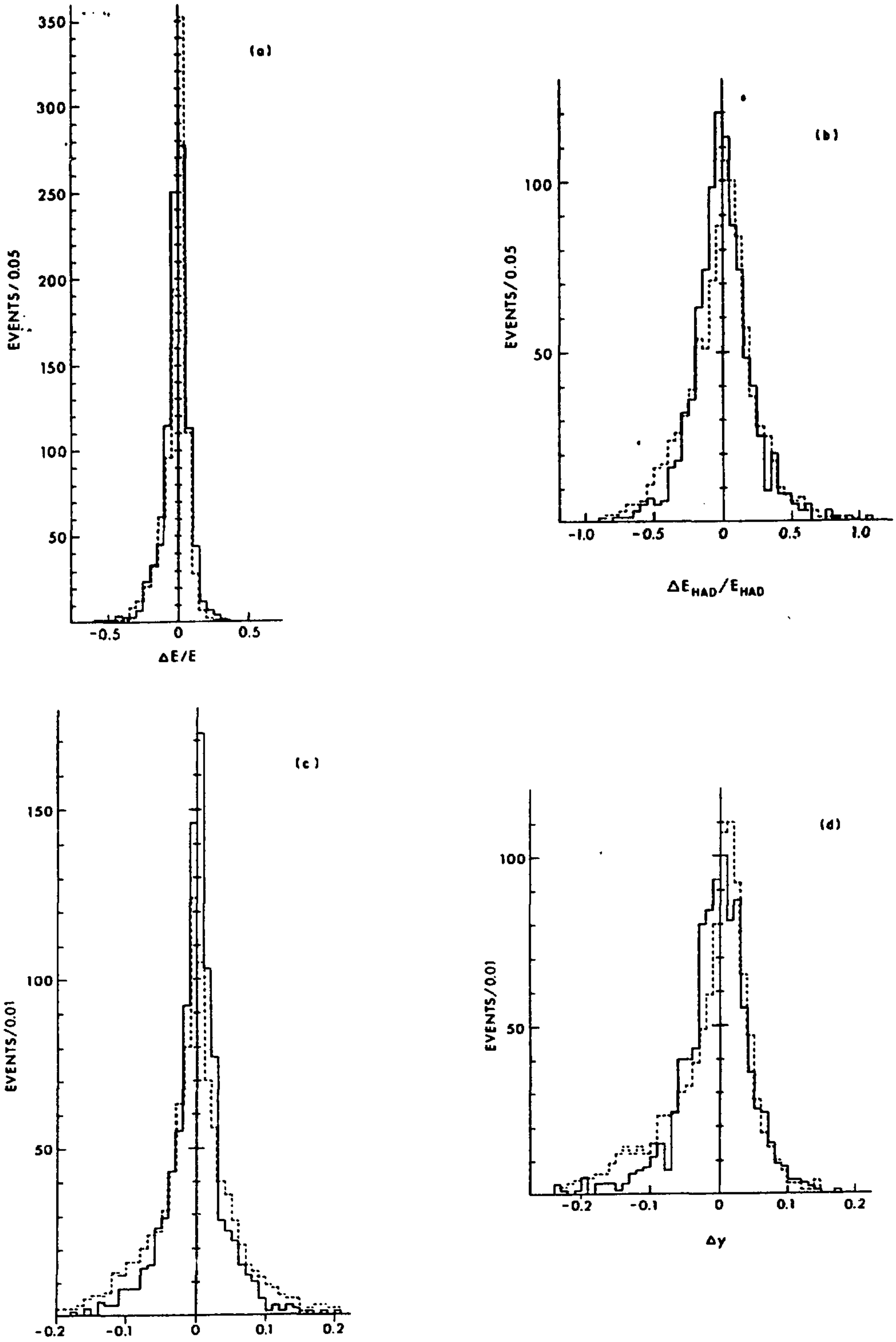

(a)
EVENTS/0.05
ΔE/E
(b)
EVENTS/0.05
ΔE_HAD/E_HAD
(c)
EVENTS/0.01
Δx
(d)
EVENTS/0.01
Δy